Interacting proteins of AMPK studied using TurboID proximity labeling technology

XIAOSHAN LIU[1*], JIEYU GUO[1*], QIONGYAO WANG[2*], WU LIU[3], YAN XUE[1], SHUANG GUO[1] and MIAO LI[4]

[1]School of Pharmacy, Hubei Key Laboratory of Diabetes and Angiopathy, Xianning Medical College, Hubei University of Science and Technology, Xianning, Hubei 437100, P.R. China; [2]Department of Oncology, Xianning Central Hospital of Hubei Province (The First Affiliated Hospital of Hubei University of Science and Technology), Xianning, Hubei 437100, P.R. China; [3]School of Basic Medical Sciences, Hubei Key Laboratory of Environmental Risks and Related Diseases Precision Control, Xianning Medical College, Hubei University of Science and Technology, Xianning, Hubei 437100, P.R. China; [4]Department of Nursing, The First Affiliated Hospital of Hainan Medical University, Haikou, Hainan 570102, P.R. China

Received September 8, 2025; Accepted March 10, 2026

DOI: 10.3892/etm.2026.13144

Abstract. In living organisms, the change in the adenosine 5'-monophosphate (AMP)/adenosine 5'-triphosphate ratio serves as a key signal regulating AMP-activated protein kinase (AMPK) activity, which is an important molecule for the control of cellular energy metabolism and serves a key role in a number of diseases, such as diabetes and myocardial infarction. To explore novel AMPK-interacting proteins and investigate their biological functions, the present study used TurboID proximity labeling in U251 cells stably expressing AMPK-TurboID. Novel AMPK-interacting proteins were explored under both normal and CCCP-treated conditions to investigate their biological functions. Stable cell lines overexpressing AMPK-TurboID were successfully established, and interacting proteins were identified through biotin labeling, silver staining and mass spectrometry analysis. Due to the involvement of AMPK in numerous metabolic pathways and the advantages of TurboID over traditional techniques, including its high temporal resolution, *in situ* labeling in living cells and its ability to capture weak and transient interactions, a number of proteins interacting with AMPK were identified. Six proteins identified by label-free MS were validated by western blotting, showing that the expression levels of menage a trois-1 and DNAJ heat shock protein family (Hsp40) member A1 (DNAJA1) closely matched the MS data. DNAJA1 was selected for further experimentation. TurboID proximity labeling, affinity purification and LC-MS/MS, western blotting, co-immunoprecipitation (co-IP) and immunofluorescence (IF) techniques demonstrated that AMPK and DNAJA1 not only interact with each other but also synergistically protect cells from apoptosis, perhaps providing a basis for targeted therapeutics (such as treatments for diabetes and myocardial infarction). The present study achieved covalent labeling of endogenous proteins located within nanometer distance of the labeling enzyme by adding a biotin-based substrate. The labeled proteins were then captured and enriched using streptavidin-coated magnetic beads for subsequent identification by MS. These MS results, combined with subsequent validation, led to the identification of DNAJA1 as a key AMPK-interacting protein that synergizes with AMPK to protect cells from apoptosis.

Correspondence to: Mrs. Shuang Guo, School of Pharmacy, Hubei Key Laboratory of Diabetes and Angiopathy, Xianning Medical College, Hubei University of Science and Technology, 88 Xianning Avenue, Xianning, Hubei 437100, P.R. China
E-mail: guoshuang@hbust.edu.cn

Dr Miao Li, Department of Nursing, The First Affiliated Hospital of Hainan Medical University, 31 Longhua Road, Longhua, Haikou, Hainan 570102, P.R. China
E-mail: 1084025840@qq.com

*Contributed equally

Abbreviations: MS, mass spectrometry; AMPK, AMP-activated protein kinase; CCCP, carbonyl cyanide 3-chlorophenylhydrazone; ATP, adenosine 5'-triphosphate

Key words: TurboID, AMPK, DNAJ heat shock protein family (Hsp40) member A1, biotin labeling, U251 cells

Introduction

Biomolecules, including proteins, nucleic acids and sugars, are important components of living organisms and perform a number of functions. The study of protein assembly, interactions and subcellular distribution is key in understanding their functions. Protein-protein interactions are the basis of cellular activities, such as replication, transcription, translation of genetic information, intercellular signaling and cellular regulation. Understanding the spatial patterns of protein localization and interactions is important in understanding cellular processes (1). The spatial distances between proteins are short and their interactions primarily rely on hydrogen, salt and hydrophobic interaction forces; therefore, we hypothesized that interacting proteins must be in close proximity to each other. Traditionally, protein interactions have been studied by affinity purification, preserving organelles or

interactions in cell lysis and purification complexes; however, this method often fails to preserve weak or transient interactions and can disrupt native protein complex conformations, making it challenging to capture physiologically relevant interactomes (2). To overcome this, proximity labeling technology combined with mass spectrometry (MS) detection is gradually becoming a more suitable method for the identification of organelle protein components and interactions (3). The principle of this technique lies in the fusion of a labeling enzyme to a targeted protein or subcellular compartment by gene fusion.

Among the currently available proximity labeling techniques, biotin ligases are the most widely used. Together with ascorbate peroxidases, they constitute the main class of labeling enzyme systems (4). Biotin ligases are engineered biotin ligase proteins that include BioID, BioID2, BASU, TurboID, miniTurbo, Split-BioID and Split-TurboID (5). The first engineered biotin ligase was BioID, which is an *Escherichia coli* BirA (bifunctional ligase or repressor) mutant with a size of 35 kDa. This enzyme has a reduced affinity for biotin-adenosine 5'-monophosphate (AMP) and can react with the primary amine of the proximal protein, leading to its covalent biotinylation (6). To address the defective target protein localization due to the large molecular weight of BioID, a new mutant (BioID2) was identified from the thermophilic bacterium *Aquifex aeolicus* with a size of 27 kDa (7). This achieves a more targeted localization and requires lower biotin concentration compared with BioID. However, both BioID and BioID2 exhibit the following limitations: First, the long labeling time (18-24 h) is not favorable for the study of short transient interacting proteins. Secondly, biotin can be actively transported into the cytoplasm of mammalian cells and freely diffuse into the nucleus; however, it has limited access to the secretory pathway, resulting in lower labeling efficiency in that compartment (8). In addition, due to the prolonged BioID labeling, biotinylation of proteins can affect their function, resulting in false positive or false negative results.

TurboID and miniTurbo were generated by targeted modifications of the BioID biotin ligase (9). Compared with BioID and BioID2, TurboID and miniTurbo require less labeling time (≤10 min) in addition to their ability to maintain catalytic activity at lower temperatures (9). The labeling principle of TurboID uses adenosine 5'-triphosphate (ATP) and biotin to generate an intermediate substance, biotin-5'-AMP, which can covalently label neighboring proteins (10), and can be used to extract or capture proteins more efficiently. Furthermore, the proximity labeling technique is now increasingly used in animal cell experiments, including protein complexes (such as nuclear pore complexes) (11), tissue proteosomes (such as mitochondrial matrix and intermembrane space) (12) and native proteomes (13,14). It has been shown that this technique not only allows for the detection of proteins that transiently interact with specific proteins in living cell (15), but also reduces the potential losses caused by traditional methods during purification and enables the precise identification of real-time (16), dynamic interacting proteins within living cells. In addition, proximity labeling technology has been extended to the study of transcriptional complexes and histone modifications (17), providing an important avenue for exploring biomolecular interactions.

AMP-activated protein kinase (AMPK) is an evolutionarily conserved serine/threonine protein kinase with AMP-dependent properties (18). As a key molecule for cells to sense external environmental changes and adjust energy metabolism, AMPK not only regulates energy metabolism at the cellular level, but also serves an important role in maintaining the energy homeostasis of the body. AMPK responds to changes in intracellular adenine nucleotide levels, being activated by an increase in AMP/ADP relative to ATP. Activation of AMPK increases the rate of catabolic (ATP-generating) pathways and decreases the rate of anabolic (ATP-utilising) pathways. In the normal physiological state, the intracellular AMP level is generally low; when the ATP level decreases after energy consumption, the AMP level and the AMP/ATP ratio increase, followed by the activation of AMPK by its upstream regulator (AMPK kinase) through phosphorylation (19). Therefore, the state of the cell can be monitored according to the concentration of ATP, ADP and AMP. A previous study hasshown that AMPK, a key regulator of energy metabolism, improves glucose regulation in type 2 diabetes through its activation by drugs such as metformin; however, its role in insulin secretion is complex and remains controversial (20). In addition, AMPK as exhibits an anti-apoptotic effect in cardiomyocytes, and its activation not only reduces myocardial energy consumption but also increases energy production, stabilizes mitochondrial membrane potential to reduce intracellular reactive oxygen species and serves a protective role against ischemia/reperfusion injury and doxorubicin-induced cardiotoxicity in the myocardium, as demonstrated in mouse models and cultured cardiomyocytes (21). Therefore, AMPK may represent a new target for the treatment of diabetes mellitus and myocardial infarction.

In recent years, AMPK has been shown to serve a role in a number of physiological and pathological conditions, with broad potential applications. Song *et al* (22) found that sleeve gastrectomy may improve renal injury in mice with hyperuricemic nephropathy by upregulating ATP binding cassette subfamily G member 2 transcription through modulation of the AMPK/nuclear factor erythroid 2-related factor 2 pathway. A study by Peng *et al* (23) revealed that the mechanistic axis glutamine hydrolysis/AMPK/succinate-CoA ligase ADP-forming subunit-β/IL-1β regulates inflammation and obesity progression in adipose tissue macrophages (ATMs). The study demonstrated that glutamine hydrolysis in ATMs serves as a key metabolic flux responsible for providing energy (ATP) and biosynthetic precursors (for example, glutamate, aspartate and TCA cycle intermediates) and that this process is associated with AMPK activity, succinate-induced IL-1β production and the development of obesity. Furthermore, Safaie *et al* (24) revealed a complex association between AMPK activation and tyrosine kinase inhibitor-induced cardiovascular toxicity, demonstrating that AMPK activation may mitigate these adverse effects. This provides a foundation for future therapeutic strategies and suggesting that AMPK activation could be key in balancing effective cancer therapy with cardiovascular health. Zhang *et al* (25) reported that succinate overload enhances susceptibility to atrial

fibrillation and remodeling by impairing AMPK signaling and mitochondrial function.

Enzyme-catalyzed proximity labeling has emerged as a new approach for studying the spatial distribution and interaction characteristics of proteins in living cells. Existing proximity labeling techniques (for example, using engineered ascorbate peroxidase and BioID) are limited by long labeling times (>18 h) (3), high reagent toxicity and poor permeability. To overcome these limitations of enzyme-catalyzed proximity labeling techniques, previous studies have employed (9,10) a novel engineered biotin ligase, TurboID, which can catalyze the conversion of biotin into biotin-5'-AMP *in vivo*. This reactive intermediate enables the efficient covalent labeling of proximal proteins, a method that is non-toxic and fast (26). TurboID can be fused to AMPK using a plasmid cloning technique, enabling TurboID-biotinylated AMPK to be readily enriched using streptavidin beads and its binding partners subsequently identified using MS.

Carbonyl cyanide 3-chlorophenylhydrazone (CCCP) is a potent mitochondrial oxidative phosphorylation uncoupling agent that acts on the inner mitochondrial membrane to make it permeable to H^+, causing depolarization of the mitochondrial membrane potential. This induces autophagy to clear the depolarized mitochondria and further promotes the mitochondrial pathway of apoptosis (27). CCCP induces DNA damage, which in turn induces p53 expression (28). It has been shown that p53 activates AMPK-dependent inhibitory pathways that attenuate the activity of mTOR complex 1 (23). Inhibition of mitochondrial depolarization by the proton carrier CCCP facilitates triggers mitophagy and induces apoptosis and autophagy (29). CCCP-induced loss of mitochondrial membrane potential and mitochondrial dysfunction not only serve as triggers for apoptosis but also act as key signals for initiating mitophagy and broader adaptive stress responses. AMPK, as a central kinase that senses cellular energy and redox status, serves a key role in coordinating metabolism and survival, particularly in responding to mitochondrial stress and initiating mitochondrial quality control (28). DNAJ heat shock protein family (Hsp40) member A1 (DNAJA1), as an Hsp70 co-chaperone, is important in maintaining mitochondrial proteostasis, protein folding and translocation (30). Therefore, the present study hypothesized that under CCCP-induced acute mitochondrial stress, AMPK activation may regulate the function of DNAJA1 (or other chaperones) through phosphorylation or other mechanisms, thereby influencing mitochondrial protein handling and stress signaling. This may offer a novel perspective for research in this field.

Therefore, in the present study, CCCP was selected as an induction factor to treat U251 astrocytes stably overexpressing the AMPK-TurboID fusion gene through lentiviral infection, enabling investigation of the AMPK interactome under energy-depleted conditions. The U251 cell line, derived from human astrocytoma, is widely used as an *in vitro* model for neurobiology research due to its well-characterized astrocytic properties, high transfection efficiency, and stable proliferation (31). Subsequently, a TurboID proximity labeling technique was used to find novel interacting proteins associated with AMPK, and label-free quantitative protein profiling was used to obtain a number of interacting proteins. Furthermore, DNAJA1 was selected for immunoprecipitation (IP) and immunofluorescence validation. In addition, AMPK and DNAJA1 were found to be jointly involved in anti-apoptotic cell death. Therefore, the present study provided a theoretical basis to explore the biological function of AMPK and the potential development of new targeted drugs.

Materials and methods

Materials. Monoclonal antibodies against Flag (cat. no. ab205606) and DNAJA1 (cat. no. ab192904), were purchased from Abcam. AMPKα2 (cat. no. A7339), BAX (cat. no. A12009), Bcl-2 (cat. no. A0208) and α-tubulin (cat. no. AC012) antibodies were purchased from ABclonal Biotech Co., Ltd. The streptavidin-peroxidase antibody (cat. no. SA00001-0) was obtained from Proteintech Group, Inc. CCCP (cat. no. C6700) was purchased from Beijing Solarbio Science & Technology Co., Ltd. PVDF membranes were obtained from MilliporeSigma. Dynabeads™ MyOne™ streptavidin C1 (cat. no. 65001), biotin (cat. no. B20656) and liposomal transfection reagent (Lipofectamine® 2000; cat. no. 11668500) were obtained from Thermo Fisher Scientific, Inc. RIPA buffer (cat. no. G2002-100ML), DAPI (cat. no. G1012-100ML) and anti-fluorescence quenching sealing agent (cat. no. G1401-25ML) were purchased from Wuhan Servicebio Technology Co., Ltd. The anti-DYKDDDDK (Flag) affinity gel (cat. no. 20585ES03), lentivirus concentration solution (cat. no. 41101ES50) and protein silver staining kit (cat. no. 36244ES25) were purchased from Shanghai Yeasen Biotechnology Co., Ltd. A DNA purification kit (cat. no. DP204) and a high purity plasmid extraction kit (cat. no. DP104) were obtained from Tiangen Biotech Co., Ltd. Lastly, inorganic salts were purchased from Sinopharm Chemical Reagent Co., Ltd.

Cell lines and culture. 293T (human embryonic kidney epithelial) and U251 (malignant astrocyte) cell lines were obtained from American Type Culture Collection. U251 and 293T cells were cultured in DMEM (Gibco; Thermo Fisher Scientific, Inc.) containing 10% FBS (Gibco; Thermo Fisher Scientific, Inc.) and 0.5% penicillin-streptomycin. All cells were cultured in a CO_2 incubator at 37˚C with 5% CO_2.

Construction of AMPK-TurboID overexpression vector. TurboID cDNA was synthesized and integrated into a plenti-cytomegalovirus (CMV)-EGFP (Beijing Tsingke Biotech Co., Ltd.) plasmid replacing the EGFP fragment (plenti-CMV-TurboID). This was conducted by Beijing Tsingke Biotech Co., Ltd. The AMPK gene was amplified using human cDNA as a template and the following primers: AMPK forward, 5'-atagaagacaccgactctagaATGGCTGAG AAGCAGAAGCAC-3'; AMPK reverse, 5'-catacgcgtgatatc cccgggACGGGCTAAAGTAGTAATCAG-3' (the lowercase letters indicate restriction enzyme sites and protective bases, and the uppercase letters indicate the gene-specific sequences that anneal to the template). The thermocycling conditions were as follows: Initial denaturation at 94˚C for 5 min; followed by 30 cycles of denaturation at 94˚C for 30 sec, annealing at 56˚C for 30 sec and extension at 72˚C for 2 min; with a final extension at 72˚C for 8 min. The plasmid plenti-CMV-TurboID was double digested using *Xba*I and *Sma*I and the AMPK fragment

was purified using a DNA purification kit and combined with the linearized plenti-CMV-TurboID plasmid. Positive clones were screened following transformation into *E. coli* TOP10 cells and selection on ampicillin (100 μg/ml)-containing LB agar plates. Plasmids were extracted using a high purity plasmid extraction kit, and then the extracted plasmids were processed through enzymatic digestion and sent to Beijing Qingke Biotechnology Co., Ltd. for sequencing of the insert. The selected plasmid was named AMPK-TurboID and was tagged with Flag.

Lentiviral packaging of AMPK-TurboID and plenti-CMV-EGFP plasmids. Firstly, 293T cells were cultured in a 10-cm dish until their cell density reached 80-90% for transfection. At the beginning of transfection, the plasmids were diluted with serum-free high-glucose medium. A total of two 1.5 ml Eppendorf (EP) tubes were prepared, one EP tube with 15 μg of psPAX2 (packaging plasmid), 6 μg of pMD2.G (envelope plasmid) and 10 μg of AMPK-TurboID (transfer plasmid) and the other EP tube with 15 μg of psPAX2, 6 μg of pMD2.G and 10 μg of plenti-CMV-EGFP (transfer plasmid). Subsequently, an appropriate amount of liposomal transfection reagent (~60 μl per 10-cm dish) was diluted with serum-free medium and incubated at room temperature for 5 min. Next, the diluted DNA plasmid and the diluted liposomal nucleic acid transfection reagent were gently mixed and incubated at room temperature for 30 min. Subsequently, the incubated DNA liposome complexes were evenly dropped into 293T cell culture dishes that had been replaced with pre-warmed complete high-glucose DMEM (containing 10% FBS) without antibiotics DMEM and incubated overnight at 37˚C in a cell culture incubator with 5% CO_2. The next day, the medium was replaced with fresh medium and incubation continued for 48-72 h when the cell supernatant was collected. The collected medium supernatant was filtered by aspiration with a 5-ml syringe onto a 0.45-mm membrane filter, after which the filtrate was mixed with lentivirus concentration reagent in a 4:1 ratio and incubated overnight at 4˚C. After incubation, the supernatant was removed by centrifugation (4˚C; 6,580 x g; 40-60 min) and fresh medium was added to the sediment and dispensed into a number of 1.5 ml EP tubes.

Construction and validation of AMPK overexpression cell lines. U251 cells were grown in 10-cm cell culture dishes and when cell confluence reached 80-90%, an appropriate number of cells ($2x10^5$) were seeded in 24-well cell culture plates. When the cell density reached 70-80%, lentivirus concentrate carrying either the AMPK-TurboID plasmid or the plenti-CMV-EGFP plasmid was dropwise added to different wells of the plate, and the cells were infected (multiplicity of infection of 10) for 6-8 h at 37˚C and replaced with fresh medium. The fluorescence intensity of plenti-CMV-EGFP plasmid-infected cell culture plates was visualized using an inverted fluorescence microscope. after 48 h. Successful infection was demonstrated when stronger fluorescence appeared. Resistance screening was performed with medium containing puromycin (1.5 μg/ml) and cell status was observed after 24-48 h. Maintenance was performed in 0.5 μg/ml puromycin. Viable cells were cultured into 12-well plates and sequentially passaged to the number of cells that met the requirements of subsequent experiments. The time interval from transduction to subsequent experiments was ~2 weeks. During this period, the cell status was observed daily and medium was renewed once every 2 days. A number of cells were used to obtain cell lysate for SDS-PAGE gel electrophoresis and determine whether stable transfection was successful. Cells stably transfected with the plenti-CMV-EGFP plasmid were named EGFP-U251 cells and cells stably transfected with the AMPK-TurboID plasmid were named AMPK-U251 cells.

Screening of AMPK biotin labeling time. AMPK-U251 cells were grown into 6-well culture plates and experiments were performed when their density reached ~80%. Cell medium was replaced with complete medium containing biotin (500 μmol/l), magnesium chloride ($MgCl_2$; 1 μmol/l) and ATP (200 μmol/l) and incubated at 37˚C, and seven labeling time gradients were set, namely 0 and 10 min, 1, 3, 6, 12 and 24 h. Cells were collected, cell lysis was performed and cell lysates were subjected to western blotting using a streptavidin-peroxidase antibody.

Western blotting. To confirm successful stable transfection, whole-cell lysates were prepared from the generated EGFP-U251 and AMPK-U251 cells, as well as control U251 cells. Cells were washed twice with ice-cold PBS and lysed in RIPA lysis buffer (cat. no. P0013B; Beyotime Biotechnology) supplemented with a protease inhibitor cocktail on ice for 30 min. The lysates were clarified by centrifugation at 12,000 x g for 20 min at 4˚C. Protein concentrations were determined using an Enhanced BCA Protein Assay Kit (cat. no. P0009; Beyotime Biotechnology). Equal amounts of protein (10 μg per lane) were denatured in 5X SDS-PAGE loading buffer at 95˚C for 10 min. The samples were then separated by SDS-PAGE on a 10% polyacrylamide gel at 120 V for 1.5 h. Following electrophoresis, the proteins were transferred onto a PVDF membrane (cat. no. IPVH00010; MilliporeSigma) using a wet transfer system at 250 mA for 150 min at 4˚C. The membrane was blocked with Quick Block™ Blocking Buffer (Beyotime Biotechnology) for 15-30 min at room temperature. Subsequently, the membrane was incubated overnight at 4˚C with primary antibodies diluted in blocking buffer. The following primary antibodies were used: Rabbit anti-AMPK polyclonal antibody (cat. no. 10929-2-AP; Proteintech Group, Inc.) and rabbit anti-FLAG polyclonal antibody (cat. no. 80801-2-RR; Proteintech Group, Inc.), both diluted at 1:1,000. GAPDH was used as a loading control. After washing three times with TBST (10 min each), the membrane was incubated with the HRP-conjugated goat anti-rabbit IgG secondary antibody (cat. no. SA00001-2; diluted at 1:5,000; Proteintech Group, Inc.) for 1 h at room temperature. Protein bands were visualized using an enhanced chemiluminescence detection reagent (cat. no. BL523A; Biosharp Life Sciences). The signals were captured using a chemiluminescence imaging system (ChemiDoc™ MP Imaging System; Bio-Rad Laboratories, Inc.). Densitometric analysis of the bands was performed using ImageJ software (Version 1.53, National Institutes of Health, Bethesda, MD, USA).

Effect of adding ATP on biotin labeling. AMPK-U251 cells were cultured into 6-well culture plates and left to reach a density of ~70-80% for subsequent experiments. The original culture medium was discarded and replaced with biotin-labeling buffer containing five varying concentrations (0, 50, 100, 200 and 500 μmol/l; 37˚C) after two washes with PBS, in order to collect sufficient labeled protein and prevent oversaturation of labeling efficiency. The biotin labeling buffer was composed of complete medium containing biotin (500 μmol/l), $MgCl_2$ (1 μmol/l) and ATP (200 μmol/l) and biotin labeling buffer without ATP had only the ATP component removed. Cells were collected, cell lysis was performed and lysates were subjected to western blotting using a streptavidin-peroxidase antibody.

TurboID-based neighboring biotin labeling technology. This method was performed with reference to that previously reported by Branon *et al* (9). The wild-type U251 cell line and AMPK-U251 cell line were grown in T75 cell culture flasks and the experiment was set up in three groups: i) Blank group, two T75 culture flasks for the wild-type U251 cell line; ii) experimental group I, two T75 culture flasks for the AMPK-U251 cell line; and iii) experimental group II, two T75 culture flasks for the AMPK-U251 cell line treated with 15 μmol/l CCCP. All three groups of cells were cultured using DMEM medium containing biotin (500 μmol/l) and MgCl2 (1 μmol/l) at 37˚C, and the cells were collected after 6 h for sample preparation.

Affinity purification of biotin-labeled proteins. Cells in the T75 cell culture flasks were collected by centrifugation (11,200 x g for 15 min at 4˚C) into 1.5-ml centrifuge tubes, resuspended by adding 1 ml of RIPA buffer (containing PMSF), and placed on ice for ~20 min for lysis. In parallel, the Dynabeads were centrifuged at 11,200 x g for 15 min at 4˚C. The supernatant was transferred to a 1.5-ml centrifuge tube. Subsequently, the streptavidin-coated magnetic beads were washed with 1 ml RIPA buffer for ~2 min at 37˚C, the supernatant was clarified by adsorption on a magnetic stand, RIPA buffer was discarded and washing was repeated 5 times at 37˚C. After the last wash, the beads were divided into three equal parts (200 μl per aliquot), and after precipitation on a magnetic stand the RIPA buffer was discarded. The protein lysate (1 ml) was added to the beads separately, placed at 4˚C and shaken slowly overnight using a 360˚ shaker. The next day, the supernatant was discarded and the samples were washed once with 1 ml potassium chloride, three times with Buffer 1 [3M NaCl 33.5 ml, 1M Tris-HCl (pH 7.4) 0.5 and 16 ml Ultrapure Water] configured in advance, once with 1 ml sodium carbonate buffer and then 2 min (maximum 3 min) with 1 ml 10% SDS, after which 1 ml RIPA buffer was added and soaked continuously for 1 min at 50˚C in a metal bath.

Subsequently, one-third of each sample was removed and processed for silver staining, while the rest of the samples were washed twice with RIPA buffer and PBS, then stored at -20˚C. Cells were counted and lysed at equal cell densities. Protein samples (10 μg per lane) were separated by 10% SDS-PAGE. Subsequent experiments were performed using a silver staining kit (fixative, sensitizing, silver staining, development and termination solutions) following the manufacturer's protocol. the gel was removed and placed in 100 ml fixative on a 60-70 rpm shaker for 20 min. The fixative was discarded and placed in 100 ml 30% ethanol on a slow shaker for 10 min. The fixative was discarded and 100 ml 30% ethanol was added with the samples shaken slowly for 10 min. The ethanol was then discarded, 200 ml deionized water was added and shaken slowly for 10 min. The water was replaced with 100 ml 1X sensitizing solution and shaken for 4-5 min. The sensitizing solution was replaced with 200 ml deionized water and shaken for 1 min, the process was repeated and the water discarded. A total of 100 ml 1X silver staining solution was added and shaken for 30-40 min. Then, 100 ml deionized water was added, shaken for 30 sec, repeated once and then the water was discarded. Subsequently, 100 ml color development solution was added and shaken until bands appeared (3-10 min). The color development solution was replaced with 100 ml termination solution and shaken for 10 min. The termination solution was discarded, 100 ml deionized water was added and shaken for 30 sec, repeated once and the water discarded. Images were captured with a camera. All incubations and washes were performed at room temperature.

Liquid chromatography-tandem MS analysis. The remaining two-thirds of the protein samples were sent to Spectrum Zhonghe (Wuhan) Life Science Technology Co., Ltd., for label-free quantitative MS (32). The LC-MS/MS analysis was performed using an Orbitrap Exploris 480 mass spectrometer coupled with an EASY-nLC 1200 liquid chromatography system (both Thermo Fisher Scientific, Inc.). Ionization was carried out in positive electrospray ionization (ESI+) mode with a spray voltage of 2,000 V. The mass spectrometer was operated in data-dependent acquisition mode, acquiring full MS scans over a mass range of 350-1,250 m/z at a resolution of 15,000, followed by higher-energy collisional dissociation (HCD) fragmentation with a normalized collision energy of 28. The ion transfer tube temperature was set to 320˚C, and the nebulizer (sheath gas) pressure and auxiliary gas flow rate were both set to 3 arbitrary units (these values are not directly provided in psi or l/min, as they are controlled by the instrument software). No multiple reaction monitoring transitions were assessed in this study, as the analysis was performed using label-free quantification.Enrichment analysis was performed on the data obtained. The online analysis tool Sangerbox (version 3.0; http://vip.sangerbox.com/home.html) was used for Gene Ontology (GO) and Kyoto Encyclopedia of Genes and Genomes (KEGG) analysis. Significantly changed proteins were identified using a threshold of FDR <0.05 and |log2FC|>1. A total of 1,045 interacting proteins in the AMPK overexpression group were selected for analysis.

Validation of protein interactions between DNAJA1 and AMPK. Protein interactions were initially verified using a co-IP assay. Wild-type U251 cells and AMPK-U251 cells were collected into EP tubes and labeled as A1 and B1, respectively. To tubes A1 and B1, 1 ml of IP lysis buffer and 10 μl of PMSF were added. The cells were then gently pipetted to disperse and placed on a rotator at 4˚C for 30 min for lysis. The lysed cells were centrifuged in a refrigerated centrifuge at 4˚C and 11,200 x g for 10 min, and protein concentrations

were determined using a BCA assay. Two additional EP tubes were labeled as A2 and B2, and 50 μl of Anti-DYKDDDDK magnetic beads were added to each tube. Subsequently, 1 ml of IP lysis buffer was added to tubes A2 and B2, and the tubes were placed on a rotator at 4˚C for 10 min to wash away impurities; this washing step was repeated twice. After discarding the IP lysis buffer from tubes A2 and B2, 900 μl of the protein lysate from tube A1 was transferred to tube A2, and the same procedure was performed for tube B1 using lysate from tube B1. Tubes A2 and B2 containing the lysate-bead mixtures were placed on a rotator at 4˚C and incubated overnight. The next day, tubes A2 and B2 were removed, the original solution was discarded, and 1 ml of PBS was added. The tubes were placed on a rotator at 4˚C for 10 min to wash; this washing step was repeated twice. After discarding the PBS from tubes A2 and B2, an appropriate amount of 1X loading buffer was added. An appropriate amount of loading buffer was also added to tubes A1 and B1. All four EP tubes were placed in a thermo mixer at 100˚C for 10 min to denature the proteins. Finally, SDS-PAGE gel electrophoresis was performed.

In a second step, AMPK-TurboID cells ($5x10^4$ cells/cm^2) were seeded in a 3.5-cm cell confocal dish, the medium was discarded when the density reached 80%, PBS added to wash the cells for 3 min and washing was repeated twice. Subsequently, 4% paraformaldehyde was added (37˚C) for 15 min to fix the cells in the dish and then discarded. PBS was added for 3 min and discarded, and washing was repeated twice. Next, 0.5% Triton X-100 was added for 20 min at room temperature and then PBS was added for 3 min and repeated twice. PBS was absorbed from the dish with absorbent paper and 200 μl of normal goat serum (cat. no. AR0009; Wuhan Boster Biological Technology, Ltd.) was added dropwise and incubated at room temperature for 30 min for blocking. The solution was removed with absorbent paper, and a primary antibody solution (2.5 μl DNAJA1 primary antibody; 1:200 dilution; 1 μl Flag; 1:500 dilution primary antibody and 500 μl primary antibody dilution) was added and incubated at 4˚C overnight. The cells were washed for 3 min with PBS twice and PBS was removed with absorbent paper. The secondary antibodies, Cy3-conjugated goat anti-mouse IgG (1:250 dilution; cat. no. A0516; Beyotime Biotechnology) and FITC-conjugated goat anti-mouse IgG (1:250 dilution; cat. no. A0568; Beyotime Biotechnology), were diluted in 250 μl of PBS and added to the cells. After incubation at room temperature for 1 h in the dark, the cells were incubated with DAPI (1 μg/ml; 37˚C) for 5 min and washed three times with PBS for 5 min. After absorbing the PBS with blotting paper, the slides were sealed with anti-fluorescent quenching agent and cells were observed under a confocal Olympus FV3000 microscope (Olympus Corporation).

Statistical analysis. Data analysis and graphing were conducted with GraphPad Prism (version 10.1.2; Dotmatics). Each group of data as the mean ± SD from three experimental replicates. Comparisons among groups were performed using one-way ANOVA followed by Tukey's honestly significant difference test. $P<0.05$ was considered to indicate a statistically significant difference.

Results

Construction of overexpression plasmids and TurboID tagging flow chart. Fig. 1A shows the composition of the AMPK-TurboID overexpression plasmid, including the target gene AMPK, the biotin labeling enzyme TurboID and the tag protein Flag, as well as two different resistance screening markers, ampicillin and puromycin, whereby ampicillin was used for the screening of positive clones in *Escherichia coli* and puromycin was used for the screening of stably transfected cells. Fig. 1B illustrates the biotin labeling experiment. First, AMPK-U251 cells that were successfully and stably transfected were placed in a biotin environment with a suitable concentration, so that free biotin could fully enter the cells. Adjacent proteins were covalently labeled with biotin by TurboID. After the protein affinity purification experiment, other proteins that were not labeled with biotin were excluded and the proteins that had been labeled with biotin were enriched. Lastly, the labeled proteins were analyzed by label-free quantitative MS.

Construction of AMPK-TurboID overexpression stable cell line. As shown in Fig. 2A, a large amount of fluorescence was observed under the microscope in plenti-CMV-EGFP-transfected 293T cells after 48 h, determining that 293T cells had been successfully transfected and the viral fluid supernatant could be collected to infect cells. Subsequently, as demonstrated in Fig. 2B, U251 cells infected with the lentivirus carrying the plenti-CMV-EGFP construct for 48 h exhibited a large amount of fluorescence, implying that the concurrent AMPK-TurboID gene was also effectively infected into U251 cells with high probability.

Validation of AMPK-TurboID overexpression in stably transduced cell lines. Comparative analysis of stably transduced AMPK-TurboID and TurboID-U251 cell lines was conducted through western blotting. Western blotting was performed with both an AMPK antibody and a Flag antibody (Fig. 2C). The results revealed that the AMPK-TurboID fusion protein showed a uniform and clear band at a molecular weight of ~97 kDa (molecular weight of AMPK, 62.3 kDa; molecular weight of TurboID, 35 kDa; Flag size was neglected), while the corresponding protein region in the TurboID-U251 cell line was blank, indicating that the stable cell line was successfully constructed.

Biotin labeling and silver staining. The results of the biotin labeling assay showed that interacting proteins of AMPK appeared after 10 min and more markedly after 1 h of labeling (Fig. 3A). To prevent oversaturation of biotin labeling, 6 h was used as the biotin labeling time of AMPK-U251 cells in the subsequent experiment. The results showed that there was some improvement in biotin labeling efficiency with the addition of ATP, however the effect was limited (groups 4-6; Fig. 3B). Considering the possible effect of the addition of ATP on the activity of AMPK, ATP was not added to the subsequent biotin-labeling buffers in the present study.

Subsequently, the U251 and AMPK-U251 cell lines underwent affinity purification and silver staining. As shown in Fig. 3C, U251 as a negative control pulled only a limited number of proteins. Since U251 cells do not express TurboID, they theoretically should not enrich biotin-labeled proteins;

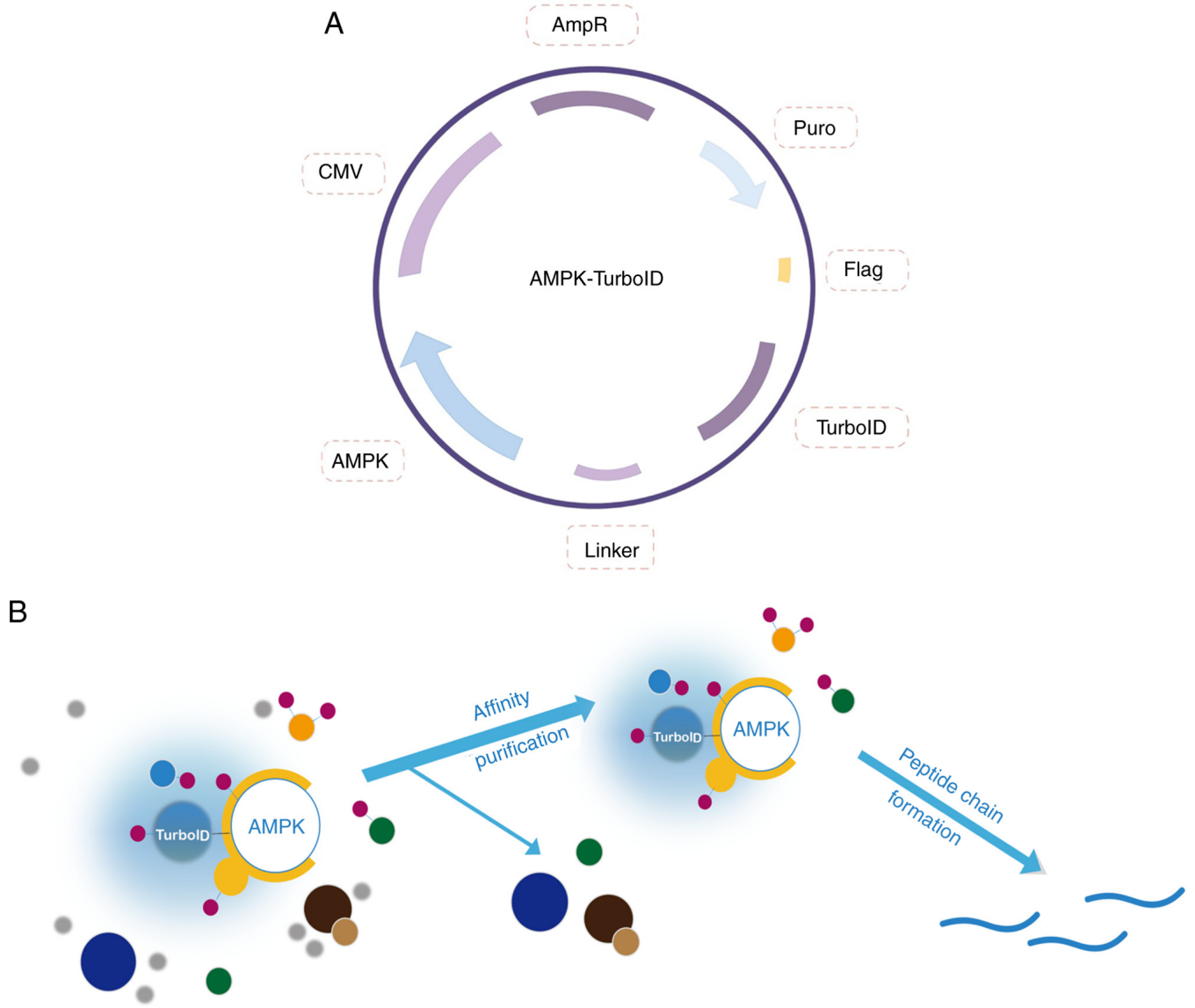

Figure 1. Construction of the overexpression plasmid and flow chart of TurboID labeling. (A) Diagram of the functional elements of the AMPK-TurboID overexpression plasmid. (B) Biotin labeling experimental workflow. AMPK, AMP-activated protein kinase.

therefore, the few protein bands observed likely represent non-specific binding or experimental background noise. Therefore these data were excluded. The remaining two sets of data indicated that AMPK overexpressing cell lines pulled a higher number of biotin-interacting proteins.

MS data analysis. Analysis of the MS data revealed a total of 1,808 non-redundant interacting proteins identified by proximity labeling across all groups after removing duplicates, with 329 proteins identified in the U251 blank group and 1,045 proteins identified in the AMPK overexpression group and 1,705 proteins in the CCCP-treated group. Furthermore, after excluding 129 proteins that were also identified in the blank group, 916 interacting proteins remained (Table SI). In addition, 1,705 proteins were identified in the CCCP-treated group and after excluding 296 proteins that were also identified in the blank group, 1,409 interacting proteins remained (Table SII).

The online analysis tool Sangerbox 3.0 was used for GO and KEGG analysis. A total of 1,045 interacting proteins in the AMPK overexpression group were selected for analysis. In the analysis of cellular components, the terms 'cytosol', 'nuclear part', 'protein-containing complex', 'nuclear lumen' and 'non-membrane-bounded organelle' were enriched (Fig. 4A). In the analysis of molecular functions, the search revealed enrichment of 'RNA binding', 'enzyme binding', 'ribonucleotide binding' and 'ATP binding' (Fig. 4B). The enrichment of 'ATP binding' reflects AMPK's function as a cellular energy sensor, while 'RNA binding' suggests a potential role in post-transcriptional regulation. In addition, a number of significantly enriched terms were identified in the analysis of biological processes, including 'organelle organization', 'positive regulation of metabolic process', 'cellular localization', 'positive regulation of macromolecule metabolic process' and 'cellular macromolecule localization' (Fig. 4C). These terms directly reflect AMPK's central role in coordinating metabolism and organelle dynamics. In the KEGG analysis, pathways that were found to be enriched included 'endocytosis', 'spliceosome', 'RNA transport', 'regulation of actin cytoskeleton',

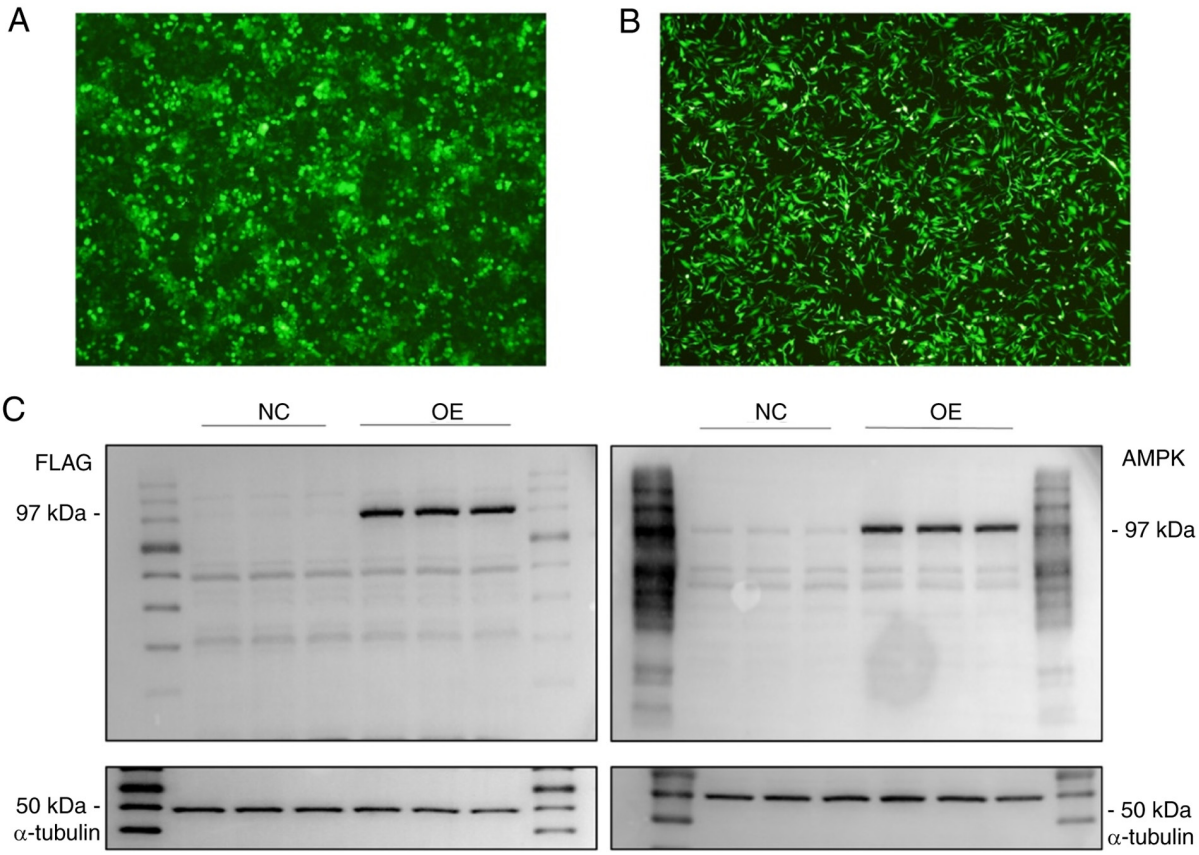

Figure 2. Fluorescence imaging and validation of the stably transfected cell lines. (A) Fluorescence image of the 293T cell line expressing plenti-CMV-EGFP. (B) Fluorescence image of the U251 cell line expressing plenti-CMV-EGFP. (C) The left image shows the levels of Flag, and the right image shows the levels of AMPK. NC, negative control (U251 cells); OE, overexpression (AMPK-TurboID overexpression cells with stable transfection); AMPK, AMP-activated protein kinase; EGFP, enhanced green fluorescent protein.

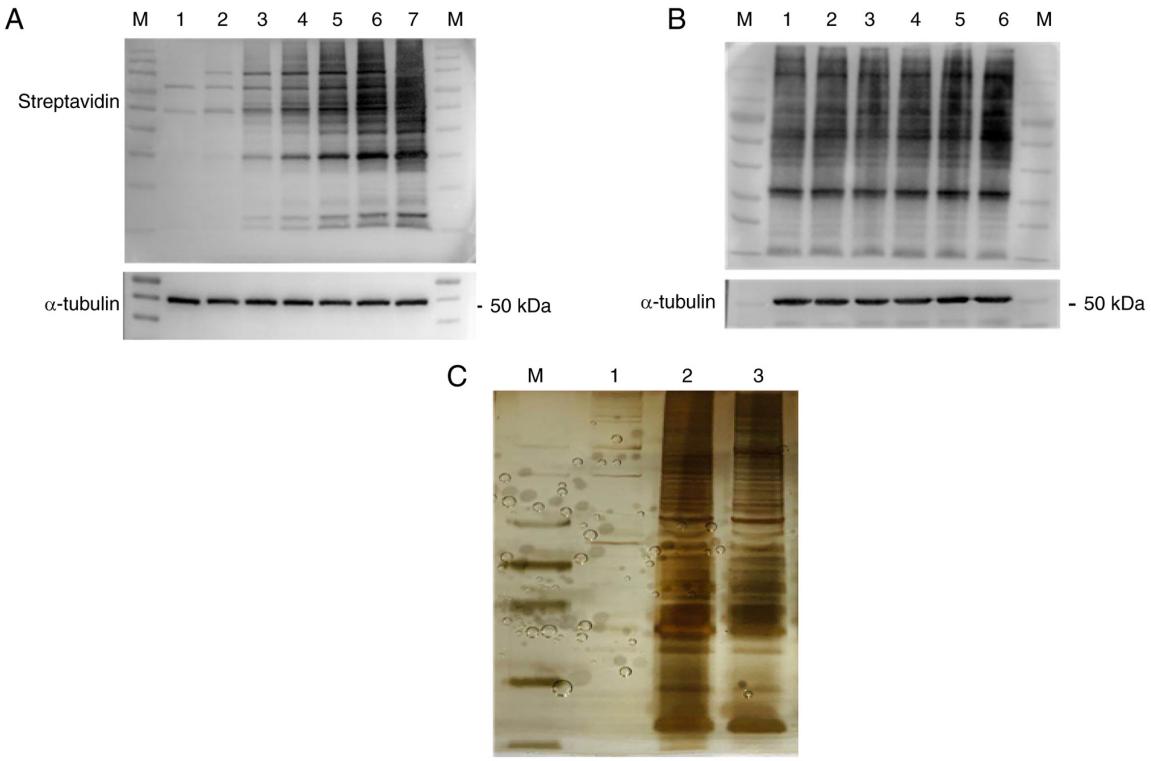

Figure 3. Biotin labeling and silver staining. (A) Biotin labeling time screening. 1, 0 min; 2, 10 min; 3, 1 h; 4, 3 h; 5, 6 h; 6, 12 h; and 7, 24 h. (B) Effect of adding ATP on biotin labeling. 1, 2, 3 indicate repeats without ATP added; 4, 5, 6 indicate repeat groups with ATP added. (C) Identification by silver staining. 1, U251; 2, AMPK-U251; 3, AMPK-U251 cells treated with carbonyl cyanide 3-chlorophenylhydrazone. M, molecular weight standard; AMPK, AMP-activated protein kinase.

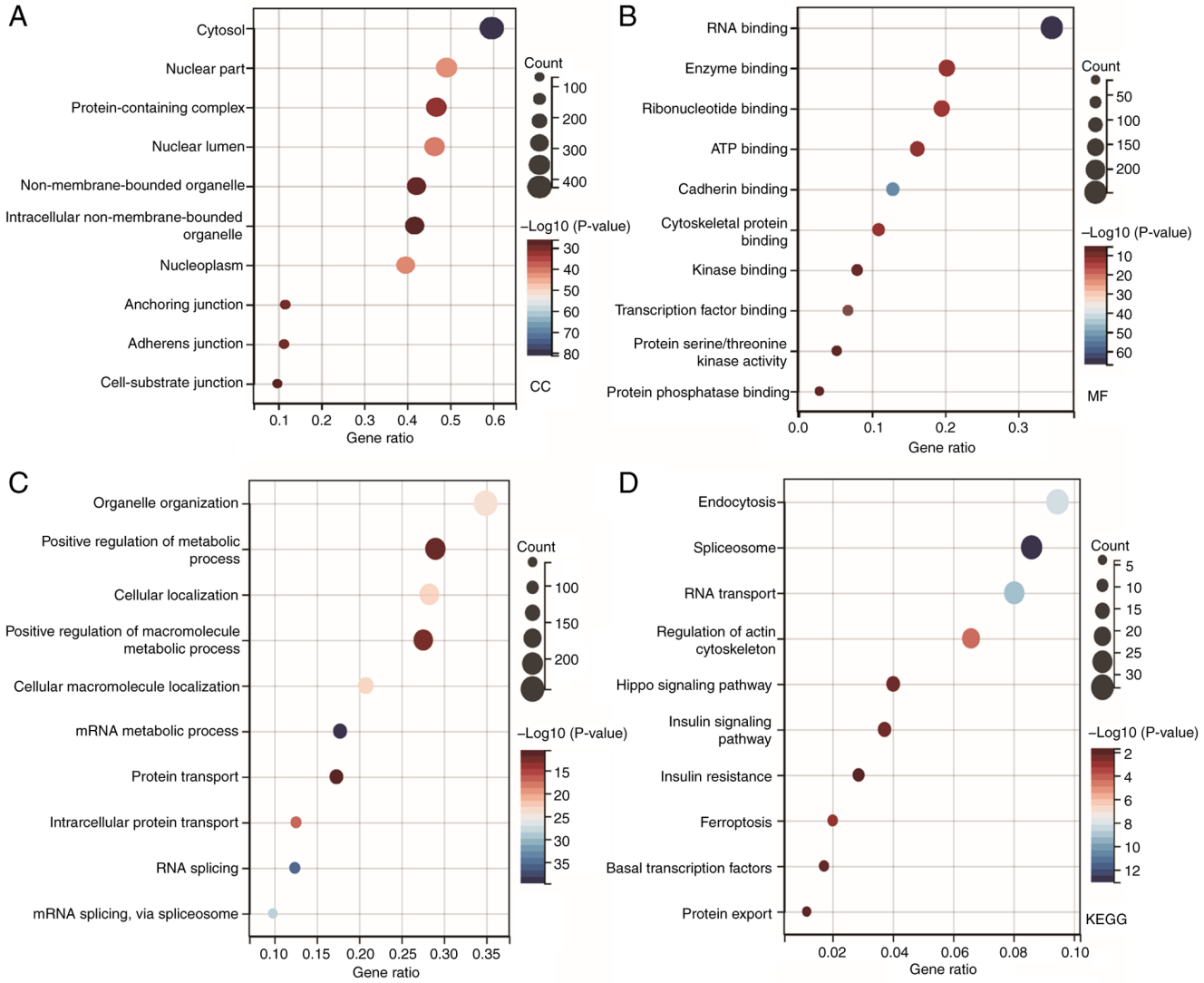

Figure 4. Analysis of AMPK interacting proteins. (A) Enriched pathways of proximate proteins of AMPK based on CC. (B) Enriched pathways of proximate proteins of AMPK group based on MF. (C) Enriched pathways of proximate proteins of AMPK group based on BP. (D) Enriched pathways of proximate proteins of AMPK group based on KEGG analysis. AMPK, AMP-activated protein kinase; KEGG, Kyoto Encyclopedia of Genes and Genomes; CC, cellular components; MF, molecular functions; BP, biological processes.

'Hippo signaling pathway', 'insulin signaling pathway', 'insulin resistance' and 'ferroptosis' (Fig. 4D).

DNAJA1 interacts with AMPK. MS data revealed that DNAJA1 is an interaction partner of AMPK. DNAJA1, a key protein in the protection against apoptosis, acts as a co-chaperone protein for heat shock protein family A member 1B and negatively regulates the transport of Bax from the cytoplasm to the mitochondria under conditions of cellular stress (33). Co-IP assays revealed that DNAJA1 interacts with AMPK. As shown in Fig. 5A, AMPK may specifically precipitate DNAJA1.

Immunofluorescence detection of the localization of AMPK and DNAJA1 in U251 cells further provided a basis for the interaction between AMPK and DNAJA1. Fig. 5B shows that both AMPK and DNAJA1 were localized in the cytoplasm, providing a spatial and temporal basis to further determine the interactions between AMPK and DNAJA1.

AMPK interacts with DNAJA1 to participate in anti-apoptosis. It has previously been established (33) that DNAJA1 is involved in the negative regulation of Bax and thus participates in the anti-apoptotic process. The present study demonstrated the existence of an interaction between AMPK and DNAJA1 and therefore hypothesized that AMPK may interact with DNAJA1 to participate in the anti-apoptotic pathway of cells. As shown in Fig. 6, the expression levels of DNAJA1 were showed a slight non-significant increase and the expression level of Bax was decreased in the AMPK overexpressing cell line compared with those in the U251 cell line, while Bcl2 expression showed no significant change, indicating that the apoptotic process may be attenuated in AMPK overexpressing cells. CCCP is a mitochondrial uncoupler that disrupts mitochondrial membrane potential and depletes cellular ATP levels, thereby inhibiting AMPK activity (34). The CCCP-treated AMPK-TurboID overexpressing cell line exhibited significantly weakened DNAJA1 and Bcl2 levels but enhanced Bax levels compared

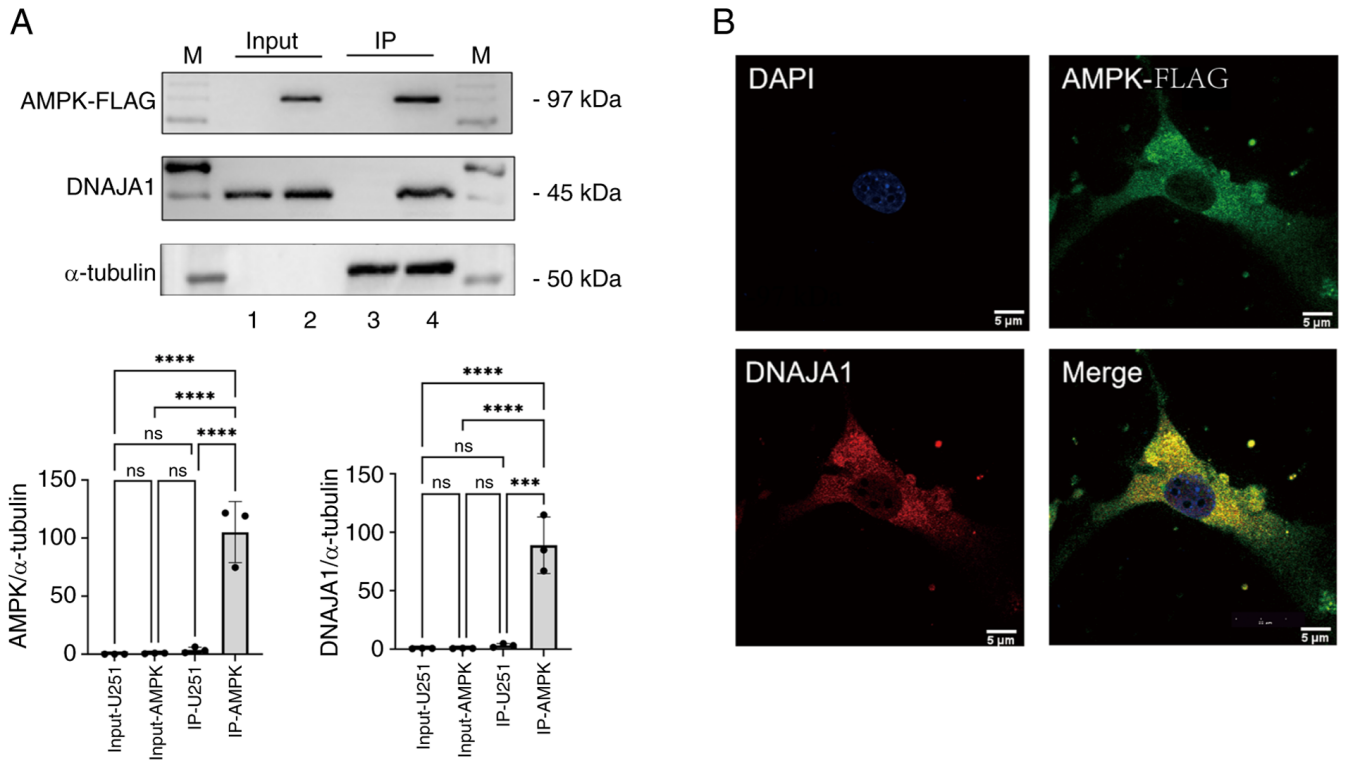

Figure 5. Validation of the interaction between AMPK and DNAJA1. (A) Co-IP was used to verify the interaction between AMPK and DNAJA1. 1, Input of U251 cell line; 2, input of AMPK overexpressing cell line; 3, co-IP eluate of U251 cell line after Flag-magnetic beads affinity adsorption; and 4, co-IP eluate of AMPK overexpressing cell line after Flag-magnetic beads affinity adsorption. (B) Immunofluorescence validation of the interaction between AMPK and DNAJA1. ***P<0.001, ****P<0.0001; ns, not significant. AMPK, AMP-activated protein kinase; DNAJA1, DNAJ heat shock protein family (Hsp40) member A1; IP, immunoprecipitation; ns, not significant; M, molecular weight standard.

with those in the AMPK overexpressing cells without CCCP treatment.

Discussion

Proteins are not only the material basis of life activities but also important components of cells, and are one of the primary regulators of physiological functions and metabolism in the human body. Proteins act in two main forms, either alone or in specific complexes with other proteins or chaperone molecules (35,36). The study of protein interactions is an important aspect of protein functional study (37). Based on the concept that interacting proteins must be in proximity to each other, proximity labeling techniques have gradually become an emerging research topic. Among them, TurboID stands out among the proximity labeling techniques due to its advantages of high catalytic activity, fast labeling, no *in vivo* toxicity and easy operation. The principle of action involves catalyzing the biotinylation of the fused protein and target proteins in a proximity-dependent manner (38). In order to consistently and stably express the target gene and study protein interactions, a stably transfected cell line was constructed in the present study. Stable overexpression of genes can overcome the disadvantage of relatively limited and uncontrollable transient overexpression (39) and increase the reproducibility of experimental results.

With regard to further advancements in MS and proteomics, Song *et al* (40) identified four potential protein biomarkers in nasal swabs for the diagnosis of coronavirus disease-19 by combining matrix-assisted laser desorption/ionization time-of-flight MS analysis with top-down proteomics techniques. Xiao *et al* (41), developed an innovative research framework by integrating targeted proteomics and metabolomics technologies, enabling the screening of potential biomarkers for the early detection of hepatocellular carcinoma. The parallel-flow projection and transfer learning across omics data method proposed by Hu *et al* (42) integrates microfluidics with deep learning, enabling deep and high-resolution spatial localization of thousands of proteins across intact tissue sections. Since relying solely on mRNA measurements risks missing important biological information, Furtwängler *et al* (43) utilized recent advances in single-cell proteomics by MS to generate an *in vivo* differentiation hierarchy dataset of >2,500 human $CD34^+$ hematopoietic stem and progenitor cells. Direct protein-level analysis is essential for comprehensive biological insights. In the present study, a similar MS-based proteomics approach, combined with TurboID proximity labeling, was employed to screen for AMPK-interacting proteins in U251 cells.

The AMPK signaling pathway is also an important research avenue. AMPK trimeric serine/threonine protein kinase is composed of a catalytic subunit (α) and two regulatory subunits (β and γ) (44), which form an enzyme regulating the general switch of cellular metabolism and maintaining the balance of nutrient supply and energy demand *in vivo* (45). Studying the interaction between AMPK and other proteins is an important step in understanding its function. It has been shown that AMPK is associated with mitochondrial fission factor (MFF), which can

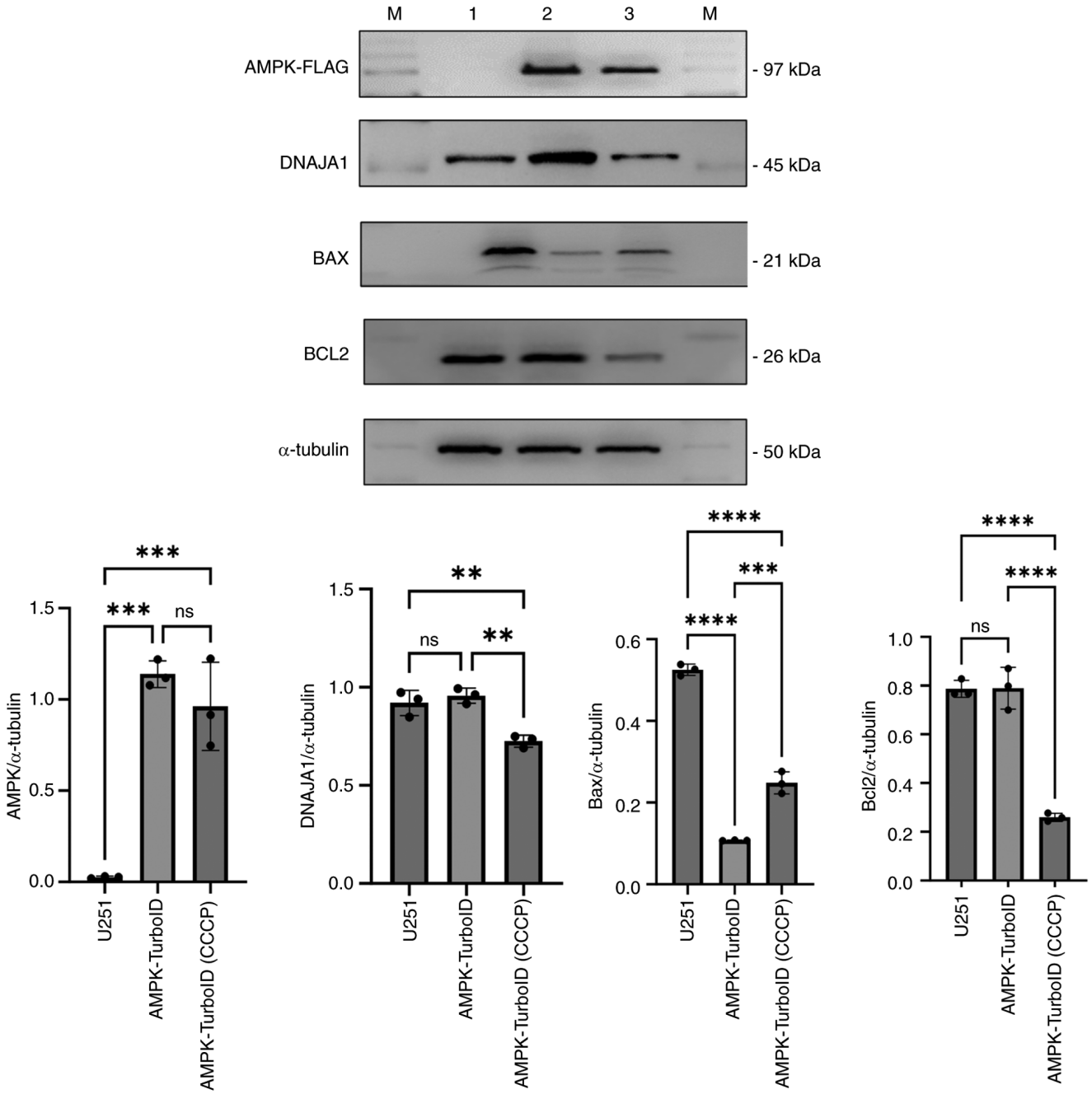

Figure 6. Western blotting validation of the interaction between AMPK and DNAJA1 in the anti-apoptosis pathway. 1, U251; 2, AMPK-U251; 3, AMPK-U251 cells treated with CCCP; AMPK, AMP-activated protein kinase; DNAJA1, DNAJ heat shock protein family (Hsp40) member A1; CCCP, carbonyl cyanide 3-chlorophenylhydrazone; ns, not significant; M, molecular weight standard. **P<0.01, ***P<0.001, ****P<0.0001; ns, not significant.

promote AMPK phosphorylation and activate mitochondrial fission. In 2022, Peng *et al* (46) demonstrated that high osmotic pressure-induced energy stress can activate the AMPK/MFF pathway, which subsequently regulates mitochondrial fission and mitophagy, contributing to the development of dry eye. Receptor-interacting protein kinase 1 (RIPK1) is a key factor in mediating cell inflammation and cell death. Zhang *et al* (47) found that AMPK may inhibit RIPK1 activation through phosphorylation at Ser415, suppressing energy stress-induced cell death. These findings provide important insights regarding the development of potential therapeutic drugs aimed at preventing ischemia-induced cell death and tissue damage. Penfluridol can activate the AMPK/FOXO3a/BIM signaling pathway and inhibit glycolysis-induced apoptosis, thereby inhibiting tumor formation. Zheng *et al* (48) found that penfluridol markedly inhibited the growth of patient-derived xenograft (PDX) tumors and the therapeutic effect of penfluridol was associated with the expression of phosphofructokinase, liver type (PFKL). PDX was subcutaneously inoculated with esophageal squamous cell carcinoma in mice, and it was found that penfluridol targeted PFKL-inhibited glycolysis and inhibited the occurrence of esophageal cancer in an AMPK/FOXO3a/BIM-dependent manner. In addition, AMPK also participates in numerous physiological processes, such as cell proliferation, metabolism (49), autophagy (50) and apoptosis (51).

Despite U251 cells being astrocytes with a metabolic environment different from that of liver, muscle, heart or

pancreatic cells, they may be still intricately associated with systemic diseases, such as diabetes. Han *et al* (52) found that the an abnormally high level of D-ribose was detected in the urine of type 2 diabetic patients, accelerated the formation of advanced glycation end-products (AGEs) in U251 and U87MG cells as well as in mouse brains, and induced the upregulation of the receptor for AGEs (RAGE). The results indicated that D-ribose-derived AGEs induced spatial cognitive impairment in mice, which was associated with the activation of RAGE-dependent inflammatory responses mediated by astrocytes. The present study focused on the screening of AMPK-interacting proteins. The human U251 astrocytoma cell line was used for cell model establishment, which exhibits a high efficiency of lentiviral infection (53,54), and resulted in the successful establishment of a stable cell line expressing the AMPK-TurboID fusion protein. This provided a solid foundation for subsequent proximity labeling and proteomic analyses. Subsequently, biotin labeling experiments were conducted and a number of proteins interacting with AMPK were found. Finally, AMPK-interacting proteins were screened by label-free MS, with GO and KEGG enrichment analysis performed on the AMPK overexpression group.

Apoptosis is a fundamental process. AMPK, a key cellular energy sensor, and DNAJA1, a co-chaperone protein, have both been implicated in the regulation of apoptosis, although their potential interplay in this process remains unclear. DNAJA1 can negatively regulate the pro-apoptotic protein Bax by inhibiting its translocation from the cytoplasm to the mitochondria during cellular stress, thus participating in the anti-apoptotic process (33). AMPK activates NF-κB to increase the expression of the anti-apoptotic protein Bcl2, thereby promoting cell survival and inhibiting apoptosis (41). The present study demonstrated the existence of an interaction between AMPK and DNAJA1 and therefore proposed the hypothesis that AMPK interacts with DNAJA1 to participate in the anti-apoptotic pathway of cells. The expression levels of Bax and Bcl2, two apoptosis markers, were compared in U251 cells, AMPK-TurboID cells and CCCP drug-treated AMPK-TurboID cells. The results showed that compared with the U251 cell line, the AMPK overexpressing cell line exhibited decreased BAX expression, indicating an attenuation of the apoptotic process. By contrast, CCCP-treated AMPK-TurboID cells exhibited significantly weaker expression of DNAJA1 and Bcl2 and enhanced expression of Bax compared with AMPK overexpressing cells without CCCP treatment, supporting the notion that AMPK can interact with DNAJA1 to inhibit apoptosis.

Lastly, despite the present study having successfully constructed an AMPK overexpression cell line, determined its interacting proteins and showed that AMPK may inhibit apoptosis, the application of the findings in treating clinical diseases where AMPK may be implicated in, such as diabetes and myocardial infarction, require further investigation.

Acknowledgements

Not applicable.

Funding

The present study was supported by The Scientific Innovation Team of Hubei University of Science and Technology (grant no. 2023T11), The Hubei Provincial Natural Science Foundation and Xianning Innovation and Development Project (grant no. 2025AFD403) and The Hubei Institute of Science and Technology Horizontal Research Project (grant nos. 2022HX135 and 2023HX188).

Availability of data and materials

The proteomics data generated in the present study may be found in the iProX database under accession number PXD044248 or at the following URL: (https://www.iprox.cn/page/project.html?id=IPX0006806000). The other data generated in the present study may be requested from the corresponding author.

Authors' contributions

XL and WL conceived and designed the study. ML, JG, YX and QW performed the experiments and acquired the data. JG, YX and QW contributed to data analysis and interpretation. JG, YX and QW prepared the figures. ML, JG and YX contributed to methodology development. QW and SG validated the experimental results. XL, ML and WL drafted the manuscript. SG, JG and YX reviewed and edited the manuscript. WL and SG supervised the project and acquired funding. All authors have read and approved the final manuscript. XL and WL confirm the authenticity of all the raw data.

Ethics approval and consent to participate

Not applicable.

Patient consent for publication

Not applicable.

Competing interests

The authors declare that they have no competing interests.

References

1. Huber LA, Pfaller K and Vietor I: Organelle proteomics: Implications for subcellular fractionation in proteomics. Circ Res 92: 962-968, 2003.
2. Wang X and Huang L: Identifying dynamic interactors of protein complexes by quantitative mass spectrometry. Mol Cell Proteomics 7: 46-57, 2008.
3. Roux KJ, Kim DI, Raida M and Burke B: A promiscuous biotin ligase fusion protein identifies proximal and interacting proteins in mammalian cells. J Cell Biol 196: 801-810, 2012.
4. Bosch JA, Chen CL and Perrimon N: Proximity-dependent labeling methods for proteomic profiling in living cells: An update. Wiley Interdiscip Rev Dev Biol 10: e392, 2021.
5. Qin W, Cho KF, Cavanagh PE and Ting AY: Deciphering molecular interactions by proximity labeling. Nat Methods 18: 133-143, 2021.
6. Samavarchi-Tehrani P, Samson R and Gingras AC: Proximity dependent biotinylation: Key enzymes and adaptation to proteomics approaches. Mol Cell Proteomics 19: 757-773, 2020.
7. Kim DI, Jensen SC, Noble KA, Kc B, Roux KH, Motamedchaboki K and Roux KJ: An improved smaller biotin ligase for BioID proximity labeling. Mol Biol Cell 27: 1188-1196, 2016.
8. Zempleni J: Uptake, localization, and noncarboxylase roles of biotin. Annu Rev Nutr 25: 175-196, 2005.

9. Branon TC, Bosch JA, Sanchez AD, Udeshi ND, Svinkina T, Carr SA, Feldman JL, Perrimon N and Ting AY: Efficient proximity labeling in living cells and organisms with TurboID. Nat Biotechnol 36: 880-887, 2018.
10. Cho KF, Branon TC, Udeshi ND, Myers SA, Carr SA and Ting AY: Proximity labeling in mammalian cells with TurboID and split-TurboID. Nat Protoc 15: 3971-3999, 2020.
11. Tourasse NJ and Li WH: Selective constraints, amino acid composition, and the rate of protein evolution. Mol Biol Evol 17: 656-664, 2000.
12. Martell JD, Deerinck TJ, Sancak Y, Poulos TL, Mootha VK, Sosinsky GE, Ellisman MH and Ting AY: Engineered ascorbate peroxidase as a genetically encoded reporter for electron microscopy. Nat Biotechnol 30: 1143-1148, 2012.
13. Mick DU, Rodrigues RB, Leib RD, Adams CM, Chien AS, Gygi SP and Nachury MV: Proteomics of primary cilia by proximity labeling. Dev Cell 35: 497-512, 2015.
14. Cho IT, Adelmant G, Lim Y, Marto JA, Cho G and Golden JA: Ascorbate peroxidase proximity labeling coupled with biochemical fractionation identifies promoters of endoplasmic reticulum-mitochondrial contacts. J Biol Chem 292: 16382-16392, 2017.
15. Huang Y, Zhai G, Li Y, Han Y, Chen C, Lu C and Zhang K: Deciphering the interactome of histone marks in living cells via genetic code expansion combined with proximity labeling. Anal Chem 94: 10705-10714, 2022.
16. Kim HB and Kim KE: Precision proteomics with TurboID: Mapping the suborganelle landscape. Korean J Physiol Pharmacol 28: 495-501, 2024.
17. Yheskel M, Sidoli S and Secombe J: Proximity labeling reveals a new in vivo network of interactors for the histone demethylase KDM5. Epigenetics Chromatin 16: 8, 2023.
18. Yan Y, Zhou XE, Xu HE and Melcher K: Structure and physiological regulation of AMPK. Int J Mol Sci 19: 3534, 2018.
19. Hardie DG, Ross FA and Hawley SA: AMPK: A nutrient and energy sensor that maintains energy homeostasis. Nat Rev Mol Cell Biol 13: 251-262, 2012.
20. Fu A, Eberhard CE and Screaton RA: Role of AMPK in pancreatic beta cell function. Mol Cell Endocrinol 366: 127-134, 2013.
21. Wang S, Song P and Zou MH: AMP-activated protein kinase, stress responses and cardiovascular diseases. Clin Sci (Lond) 122: 555-573, 2012.
22. Song K, Kong X, Zhang Z, Xian Y, He M, Zhang Y, Liao X, Huang Z, Kang A, Xiao D and Ren Y: Sleeve gastrectomy ameliorates renal injury in obesity-combined hyperuricemic nephropathy mice by modulating the AMPK/Nrf2/ABCG2 pathway. Sci Rep 14: 22834, 2024.
23. Peng C, Jiang H, Jing L, Yang W, Guan X, Wang H, Yu S, Cao Y, Wang M, Ma H, *et al*: Macrophage SUCLA2 coupled glutaminolysis manipulates obesity through AMPK. Nat Commun 16: 1738, 2025.
24. Safaie N, Idari G, Ghasemi D, Hajiabbasi M, Alivirdiloo V, Masoumi S, Zavvar M, Majidi Z and Faridvand Y: AMPK activation; a potential strategy to mitigate TKI-induced cardiovascular toxicity. Arch Physiol Biochem 131: 329-341, 2025.
25. Zhang Y, Gong H, Jin L, Liu P, Fan J, Qin X and Zheng Q: Succinate predisposes mice to atrial fibrillation by impairing mitochondrial function via SUCNR1/AMPK axis. Redox Biol 81: 103576, 2025.
26. Zhang Y, Li Y, Yang X, Wen Z, Nagalakshmi U and Dinesh-Kumar SP: TurboID-based proximity labeling for in planta identification of protein-protein interaction networks. J Vis Exp: 10.3791/60728, 2020.
27. de Graaf AO, van den Heuvel LP, Dijkman HB, de Abreu RA, Birkenkamp KU, de Witte T, van der Reijden BA, Smeitink JA and Jansen JH: Bcl-2 prevents loss of mitochondria in CCCP-induced apoptosis. Exp Cell Res 299: 533-540, 2004.
28. Kane MS, Paris A, Codron P, Cassereau J, Procaccio V, Lenaers G, Reynier P and Chevrollier A: Current mechanistic insights into the CCCP-induced cell survival response. Biochem Pharmacol 148: 100-110, 2018.
29. Han YH, Kim SH, Kim SZ and Park WH: Carbonyl cyanide p-(trifluoromethoxy) phenylhydrazone (FCCP) as an O2(*-) generator induces apoptosis via the depletion of intracellular GSH contents in Calu-6 cells. Lung Cancer 63: 201-209, 2009.
30. He Y and Wang Z: The roles of HSP40/DNAJ protein family in neurodegenerative diseases. Zhejiang Da Xue Xue Bao Yi Xue Ban 51: 640-646, 2022.
31. Roscoe JA, Gorin FA and Tait RC: Human astrocytoma U251 RNA and genomic brain glycogen phosphorylase sequences. Brain Res Mol Brain Res 10: 273-275, 1991.
32. Su Y, Guo Y, Guo J, Zeng T, Wang T and Liu W: Study of FOXO1-interacting proteins using TurboID-based proximity labeling technology. BMC Genomics 24: 146, 2023.
33. Gotoh T, Terada K, Oyadomari S and Mori M: hsp70-DnaJ chaperone pair prevents nitric oxide- and CHOP-induced apoptosis by inhibiting translocation of Bax to mitochondria. Cell Death Differ 11: 390-402, 2004.
34. Barner HB, Labovitz AJ and Fiore AC: Prosthetic valves for the small aortic root. J Card Surg 9 (2 Suppl): S154-S157, 1994.
35. Mitchem MM, Shrader C, Abedi E and Truman AW: Novel insights into the post-translational modifications of Ydj1/DNAJA1 co-chaperones. Cell Stress Chaperones 29: 1-9, 2024.
36. Liu G, Wong L and Chua HN: Complex discovery from weighted PPI networks. Bioinformatics 25: 1891-1897, 2009.
37. Li XL, Foo CS and Ng SK: Discovering protein complexes in dense reliable neighborhoods of protein interaction networks. Comput Syst Bioinformatics Conf 6: 157-168, 2007.
38. Zhang Y, Song G, Lal NK, Nagalakshmi U, Li Y, Zheng W, Huang PJ, Branon TC, Ting AY, Walley JW and Dinesh-Kumar SP: TurboID-based proximity labeling reveals that UBR7 is a regulator of N NLR immune receptor-mediated immunity. Nat Commun 10: 3252, 2019.
39. Hua F, Mu R, Liu J, Xue J, Wang Z, Lin H, Yang H, Chen X and Hu Z: TRB3 interacts with SMAD3 promoting tumor cell migration and invasion. J Cell Sci 124: 3235-3246, 2011.
40. Song R, Li D, Hao X, Lyu Q, Ma Q, Chen X and Qiao L: MALDI-TOF MS analysis of nasal swabs for the characterization of patients infected with SARS-CoV-2 Omicron. VIEW 5: 20240015, 2024.
41. Xiao J, Liu H, Yao J, Yang S, Shen F, Bu K, Wang Z, Liu F, Xia N, Yuan Q, *et al*: The characterization of serum proteomics and metabolomics across the cancer trajectory in chronic hepatitis B-related liver diseases. VIEW 5: 20240031, 2024.
42. Hu B, He R, Pang K, Wang G, Wang N, Zhu W, Sui X, Teng H, Liu T, Zhu J, *et al*: High-resolution spatially resolved proteomics of complex tissues based on microfluidics and transfer learning. Cell 188: 734-748.e22, 2025.
43. Furtwängler B, Üresin N, Richter S, Schuster MB, Barmpouri D, Holze H, Wenzel A, Grønbæk K, Theilgaard-Mönch K, Theis FJ, *et al*: Mapping early human blood cell differentiation using single-cell proteomics and transcriptomics. Science 390: eadr8785, 2025.
44. Herzig S and Shaw RJ: AMPK: Guardian of metabolism and mitochondrial homeostasis. Nat Rev Mol Cell Biol 19: 121-135, 2018.
45. Viollet B and Andreelli F: AMP-activated protein kinase and metabolic control. Handb Exp Pharmacol: 303-330, 2011.
46. Peng: Erratum in: AMPK/MFF activation: role in mitochondrial fission and mitophagy in dry eye. Invest Ophthalmol Vis Sci 63: 24, 2022.
47. Zhang T, Xu D, Trefts E, Lv M, Inuzuka H, Song G, Liu M, Lu J, Liu J, Chu C, *et al*: Metabolic orchestration of cell death by AMPK-mediated phosphorylation of RIPK1. Science 380: 1372-1380, 2023.
48. Zheng C, Yu X, Liang Y, Zhu Y, He Y, Liao L, Wang D, Yang Y, Yin X, Li A, *et al*: Targeting PFKL with penfluridol inhibits glycolysis and suppresses esophageal cancer tumorigenesis in an AMPK/FOXO3a/BIM-dependent manner. Acta Pharm Sin B 12: 1271-1287, 2022.
49. Xu J, Ji J and Yan XH: Cross-talk between AMPK and mTOR in regulating energy balance. Crit Rev Food Sci Nutr 52: 373-381, 2012.
50. Gwinn DM, Shackelford DB, Egan DF, Mihaylova MM, Mery A, Vasquez DS, Turk BE and Shaw RJ: AMPK phosphorylation of raptor mediates a metabolic checkpoint. Mol Cell 30: 214-226, 2008.
51. Zhang MH, Fang XS, Guo JY and Jin Z: Effects of AMPK on apoptosis and energy metabolism of gastric smooth muscle cells in rats with diabetic gastroparesis. Cell Biochem Biophys 77: 165-177, 2019.
52. Han C, Lu Y, Wei Y, Wu B, Liu Y and He R: D-ribosylation induces cognitive impairment through RAGE-dependent astrocytic inflammation. Cell Death Dis 5: e1117, 2014.
53. Liang D, Song Y, Fan G, Ji D, Zhang T, Nie E, Liu X, Liang J, Yu R and Gao S: Effects of long form of CAPON overexpression on glioma cell proliferation are dependent on AKT/mTOR/P53 signaling. Int J Med Sci 16: 614-622, 2019.
54. Li GH, Wei H, Chen ZT, Lv SQ, Yin CL and Wang DL: STAT3 silencing with lentivirus inhibits growth and induces apoptosis and differentiation of U251 cells. J Neurooncol 91: 165-174, 2009.

Copyright © 2026 Liu et al. This work is licensed under a Creative Commons Attribution-NonCommercial-NoDerivatives 4.0 International (CC BY-NC-ND 4.0) License.